

Carbon-based light emitting defects in different layers of hexagonal boron nitride

Ignacio Chacón and Andrea Echeverri

Departamento de Física, Facultad de Ciencias, Universidad de Chile. Santiago, Chile

Carlos Cárdenas and Francisco Muñoz

*Center for the Development of Nanoscience and Nanotechnology (CEDENNA), Santiago, Chile and
Departamento de Física, Facultad de Ciencias, Universidad de Chile. Santiago, Chile*

(Dated: December 24, 2024)

Substitutional carbon defects in hexagonal boron nitride (hBN) have garnered significant interest as single photon emitters (SPEs) due to their remarkable optical and quantum properties. An intriguing property of these defects is that they can be spin-active ($S \geq 1$), even if weakly interacting. Employing density functional theory (DFT) calculations, we demonstrate that two monomers of C-based defects of the same species can exhibit a stable triplet spin state at room temperature, even when they are separated $\lesssim 1$ nm, if they reside in different layers. The zero-phonon line (ZPL) energy of C defects in different layers lies within 1.6 – 2.2 eV range. Also, we found defects that deviate from the typical phonon replica patterns, potentially explaining the observed phonon replicas in yellow emitters in hBN.

I. INTRODUCTION

Hexagonal boron nitride (hBN) is a layered material that can be exfoliated down to the monolayer. It has garnered attention for hosting single photon emitters [1–3]. Many of these defects have been associated with substitutional carbon defects [1, 4–13], even though other options have been proposed [14–16]. Due to its large bandgap, close to 6 eV, defects incorporated within the crystal can introduce new energy levels within the gap [17, 18]. Consequently, electronic transitions give rise to SPEs exhibiting characteristics such as bright photons, a commendable coherence time [19], even at room temperature, and in some cases, they are spin-active (triplet or higher spin state) defects [20–23]. These properties are crucial for quantum technologies in communication, computation, metrology, sensing, imaging, etc. [24–30]. Therefore, the search for these types of defects is relevant, considering the scarcity of substitutional spin-active carbon defects, such as $C_N C_N$ [31], $(C_N)_3 C_B$ and $(C_B)_3 C_N$ [32, 33]. It is worth mentioning that vacancy-based SPEs in hBN are an active research field, as they often are spin-active [34–37].

Substitutional C defects behave as donors (C_B), acceptors (C_N), donor-acceptor pairs, or more complex arrangements [38, 39]. Each C defect contributes a single electron and one defect state (spin up and down) within the hBN band gap. The 4.1 eV emission line has been identified as two adjacent $C_N C_B$ defects [7], often denoted as C_2 . If the same C_N – C_B pair is in the same layer but separated by some distance, the emission energy decreases to the visible range [25, 40]. The ground state is likely spinless if the number of C_N and C_B is the same. Otherwise, the system can have a non-zero net spin. There are experimental findings of emissions attributed to C defects, even though the actual C defect has not been identified [20, 41]. One possible explanation, fitting with the available results, is weakly coupled $S = 1/2$ defects [42].

This article aims to investigate SPEs when forming a C dimer but residing in different hBN layers. Such a possibility has not been addressed before, even though defects comprising an interstitial C atom have been considered [43]. The paper is structured as follows: Section II details the methods employed for the calculations, Section III presents our main results, including the SPE's spin state - likely to be a triplet - and their photoluminescence spectra. Finally, Section IV explains the large energy difference between triplet and singlet states for some dimers, the phonon sidebands shape, and we relate our findings to experimental results on spin-active SPEs.

II. METHODOLOGY

A. Computational Methods

We used density functional theory (DFT) as implemented in the Vienna ab initio simulation package (VASP) [44–47]. A 7×7 hexagonal supercell was employed together with a single k-point (Γ). We used an hBN bilayer to simulate defects in adjacent layers. If the defects are in non-adjacent layers, we used a hBN trilayer. The connection with the bulk is almost immediate; the additional layers should have (*i*) a lesser effect on the ZPL energy due to enhanced screening [48–50] and a shift in the ZPL due to electrostatic potential [51]. We used the AA' stacking (B, N atoms on top of N, B), as found in most hBN samples [52].

The kinetic energy cutoff was set to 500 eV. PyProcar [53, 54] was used for the analysis of the results, and VESTA for visualization [55].

We used the SCAN exchange-correlation functional [56] to relax the hBN structure and to calculate phonons. Although this functional can provide an accurate description of the geometry, it could fail to accurately describe the defect levels [57]. Once the geometry was obtained with SCAN, we used the Heyd-Scuseria-Ernzerhof

(HSE06) functional to obtain the energies and the optical transitions at that geometry [58, 59]. This procedure was used for the ground and excited states. To study the excited state of each configuration, the Δ SCF method was used [60, 61]. This method has a problem of correctly describing the excited state, and there are some corrections to improve the ZPL value [7, 62]. The most interesting systems in our study have a triplet ground state and involve transitions with the valence or conduction bands, so getting the correct Slater determinant of the excited state is more involved. In the Supplementary Material, we bound this error in the ZPL energy to 0.2 eV or lower. In all cases, we restricted our study to neutral defects [32].

The formation energy of a defect was calculated by using

$$H_f(D) = E_{tot}(D) - E_{hBN} - n_C \mu_C - n_B \mu_B - n_N \mu_N, \quad (1)$$

where the $H_f(D)$ is the formation energy of a defect D , $E_{tot}(D)$ is the defect's energy, E_{hBN} is the energy of a pristine hBN bi- or tri-layer, n_X is the number of a specific atom $X = C, B, N$ which is added ($n > 0$) or removed ($n < 0$) from the defectless hBN system, and μ_X is the chemical potential of a X atom.

The chemical potentials in Eq.(1) depend on the experimental growth conditions of hBN. Bounds on the values of the chemical potentials of N and B can be established by ab initio thermodynamics method [63]. In this approach, it is assumed that the growth is a process in thermodynamic equilibrium and that the hBN serves as a reservoir of N and B. Therefore, the chemical potentials of B and N are not independent but linked by the formation enthalpy of hBN with respect to bulk B and gaseous N_2 ($\mu_B + \mu_N = \Delta H_f(BN) = -2.6$ eV/formula unit) [64, 65]. Hence, two bounds are in order. The N-poor condition in which $\min(\mu_N) = \Delta H_f(BN) + 1/2\mu_{N_2}^{gas}$, and the N-rich condition in which $\min(\mu_B) = \Delta H_f(BN) + \mu_B^{bulk}$ [5]. The chemical potential of carbon is taken as the C-rich bound such that $\mu_C^{graphite}$.

To calculate the phonon sideband of photoluminescence spectra, we used the method developed by Alkauskas *et al.* [66]. In summary, the phonons (assumed to be the same in the ground and excited states) are expanded into generalized coordinates q_k , resonating with the rearrangement upon emission.

$$q_k = \sum_{\alpha} \sqrt{m_{\alpha i}} (R_{e,\alpha i} - R_{g,\alpha i}) \Delta r_{k,\alpha i}, \quad (2)$$

where α , i , and k denote atoms, Cartesian coordinates, and the vibrational mode, respectively. R_e and R_g are the positions in excited and relaxed states, respectively. m_{α} is the atom's mass. Finally, Δr_k is the unitary vector for the k -th vibrational mode. Thus, we can obtain the partial Huang-Rhys factor S_k , representing the number of phonons of the phonon k :

$$S_k = \frac{\omega_k q_k^2}{2\hbar}, \quad (3)$$

where ω_k is the frequency of the phonon k -th vibrational mode and \hbar is the Planck Constant. From here, the optical spectral function and the phonon sideband can be directly determined [66]. The only free parameter is a thermal-like broadening of S_k , which we set to 25 meV (room temperature).

III. RESULTS

All of the defects studied are substitutional C-dimers, with both C atoms in different layers. The cases of $C_N C_B$, $C_N C_N$ and $C_B C_B$ were studied. In all dimers, the C atom in the bottom layer was kept fixed while we changed the position of the C atom in the top layer, see Fig. 1A. For clarity, we labeled the in-plane position (d) of one C atom with respect to the other with the letters 'a'-'g'. In the configuration 'a', both C atoms are on top of each other. The in-plane projection of the C-C distance is in Table I. The C atoms can belong to adjacent layers ($h = 1$) or can be separated by an inner layer ($h = 2$); see Fig. 1B-C. Thus, a given dimer defect can be identified by $C_X C_Y-(d, h)$, with $X, Y = \{B, N\}$.

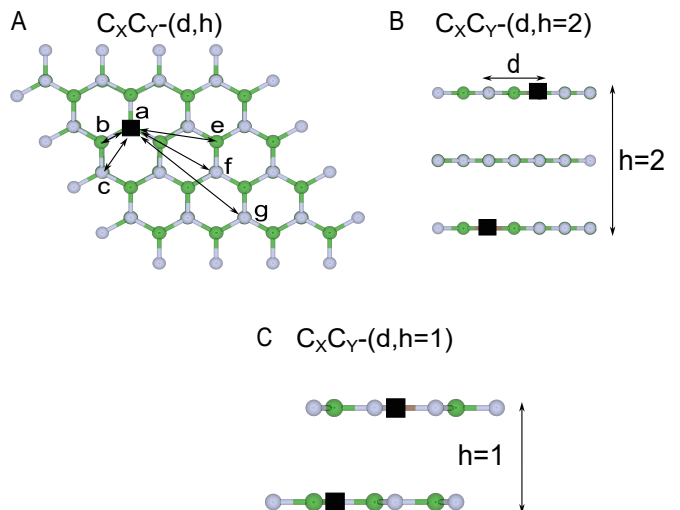


FIG. 1. Geometry of the studied defects, neutral dimers $C_X C_Y$ with $X, Y = \{N, B\}$. The defects are separated by an in-plane distance d plus an out-of-plane distance h . Panel A shows d for the defects studied and the labels used to identify them. One C atom is at the black square, and the other is at the end of the arrow. Table I gives the in-plane distance for each label of d . Panels B and C show the out-of-plane distance h , with $h = 1$ if the C atoms (black squares) are in adjacent layers and $h = 2$ when there is an hBN among the defect atoms. The different colors of the hBN lattice represent B and N atoms without specifying them (*i.e.* if the C atom in panel A is C_B , N is green; if the C atom is C_N , B is green).

Almost all configurations with C defects of the same species, *i.e.* $C_N C_N$ and $C_B C_B$, have a triplet ground state ($S = 1$) regardless of their relative position or whether they belong to adjacent layers or not. As shown

Label	Distance d (Å)	Distance C-C (Å)	
		$h = 1$	$h = 2$
a	0	3.28	6.68
b	1.45	3.93	6.85
c	2.50	4.09	7.16
e	3.82	4.46	7.74
f	4.31	-	7.97
g	6.62	-	9.44

TABLE I. The in-plane component of the distance, d , and the total distance for each pair of defects $C_X C_Y-(d, h)$. The labels are defined in Fig. 1.

in Fig. 2, the triplet is approximately 0.5 eV more stable than the singlet state; these defects will remain spin-active well above room temperature. The only exception is $C_N C_N-(b, 1)$. In this particular defect, both C_N atoms attract each other, moving out of the plane, and they form a covalent bond resembling a sp^3 hybridization.

On the other hand, for defects of the type $C_N C_B$, the ground state is always a singlet. In Section IV, we discuss why the singlet and triplet spin states are favored for different defect types.

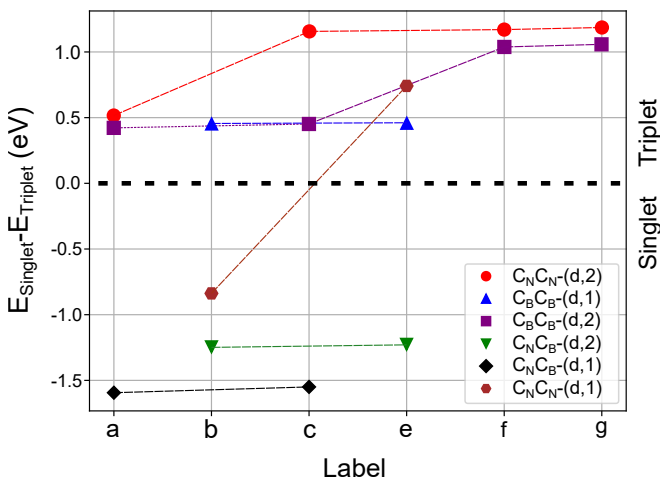


FIG. 2. Energy difference between the singlet and triplet state of each configuration. The red, blue, purple, green, black and brown markers are the $C_N C_N-(d, 2)$, $C_B C_B-(d, 1)$, $C_B C_B-(d, 2)$, $C_N C_B-(d, 2)$, $C_N C_B-(d, 1)$ and $C_N C_N-(d, 1)$, respectively. A positive (negative) value means a favorable triplet (singlet) state.

The formation energy of the $C_X C_Y$ defects is provided in Table II. Regardless of whether the defects reside in the same or different layers [31], the formation energy is primarily determined by the environment (*i.e.* the chemical potential). In the most favorable environment (N-rich for $C_B C_B$, N-poor for $C_N C_N$), $H_f \sim 3.5$ eV. Conversely, H_f increases significantly to 8.5-9.0 eV in the least favorable environment. Also, details such as the C-C distance d have a minimal effect on the formation energy. The only exception is $C_N C_N-(b, 1)$ where a covalent C-C bond develops. Note that this defect has the smallest formation

TABLE II. Formation energy H_f of the different defects studied. They are reported for two extreme environments, N-poor and N-rich.

Configuration	H_f (eV)	
	N-poor	N-rich
$C_B C_B-(b, 1)$	8.65	3.45
$C_B C_B-(e, 1)$	8.66	3.46
$C_B C_B-(a, 2)$	8.60	3.40
$C_B C_B-(c, 2)$	8.73	3.53
$C_B C_B-(f, 2)$	8.59	3.39
$C_B C_B-(g, 2)$	8.75	3.55
$C_N C_N-(b, 1)$	2.80	8.00
$C_N C_N-(e, 1)$	3.67	8.87
$C_N C_N-(a, 2)$	3.65	8.85
$C_N C_N-(c, 2)$	3.63	8.83
$C_N C_N-(f, 2)$	3.66	8.86
$C_N C_N-(g, 2)$	3.65	8.85
$C_N C_B-(a, 1)$	4.50	4.50
$C_N C_B-(c, 1)$	4.47	4.47
$C_N C_B-(b, 2)$	4.90	4.90
$C_N C_B-(e, 2)$	4.94	4.94

energy among all $C_N C_N$ defects, which is coherent with a partial covalent bond between both C atoms.

Instead, for $C_B C_N$, the formation energies are over ~ 4.5 eV. This is substantially larger than the dimer C_2 (*i.e.* C_N , C_B adjacent, in the same layer), with $H_f \approx 2.1$ eV [32]. As a comparison, topological $C_N C_B$ defects (*i.e.* Stone-Wales-like) have a formation energy even higher than the $C_N C_B$ defects studied here [67], but in these defects H_f decreases quickly with strain. Indeed, biaxial strain can substantially lower the relative formation energy of C_B or C_N depending on whether it is compressive or tensile [68]. While a large strain is not expected to be present in the bulk, C defects can act as stress valves near grain boundaries [67]. The thermal stability of C defects is determined not only by H_f but also by the energy barriers preventing them from migrating. Babar *et al.* [67] calculated the barrier energy separating a Stone-Wales C_2 dimer from the standard C_2 dimer; it surpasses 6 eV, as strong covalent bonds need to be broken. In the case of the $C_X C_Y-(d, h)$, the same applies, and we do not expect any migration induced by temperature.

The ZPL energy for defects with triplet ground state, $C_N C_N$ and $C_B C_B$, is shown in Fig. 3. When an intermediate layer of hBN separates C atoms, the value of ZPL seems to quickly converge to ~ 2.2 eV for $C_N C_N$ and ~ 1.9 eV for $C_B C_B$. When the C atoms are on top of each other or very close, the value of the ZPL decreases. As $C_N C_N-(b, 1)$ has a C-C bond, breaking would require a photon energy much larger than the hBN band gap; hence we didn't calculate its optical excitation. The donor-acceptor-like defects, $C_N C_B-(d, h)$ have a ZPL ~ 1.6 eV, which almost coincides with the ZPL of non-adjacent $C_N C_B$ when residing in the same layer [25].

Two types of photoluminescence spectra were found, see Fig. 4A. The one associated with the defect $C_B C_B-$

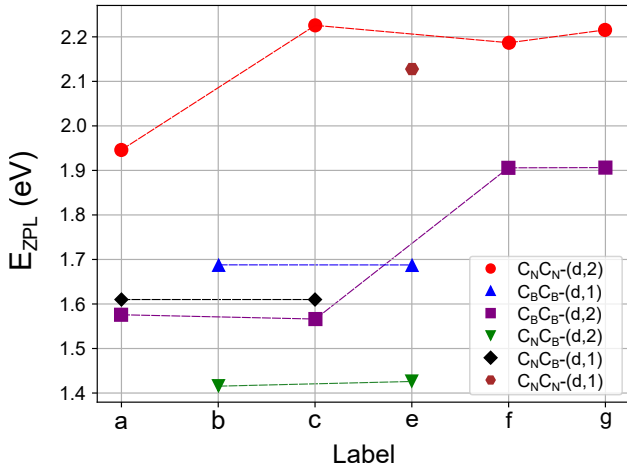


FIG. 3. ZPL Energy of the configurations. The colors red, blue, purple, green, black and brown represent the defects $C_N C_N-(d, 2)$, $C_B C_B-(d, 1)$, $C_B C_B-(d, 2)$, $C_N C_B-(d, 2)$, $C_N C_B-(d, 1)$, and $C_N C_N-(d, 1)$, respectively.

(c, 2) represents most of the defects studied here; there are high-energy phonon replicas as typically found in C-based defects in hBN. However, there is one exception, $C_B C_B-(a, 2)$, with prominent phonon replicas at 62 meV. In the next section, we will discuss the origin of both types of phonon sidebands found.

IV. DISCUSSION

A. Triplet or singlet spin ground state

Almost regardless of distances or whether defects belong to adjacent layers or are separated by an additional hBN layer, defects of the same type (*i.e.* $C_B C_B$, $C_N C_N$) have a triplet ground state, well separated in energy from the singlet state ($\gtrsim 0.5$ eV). The same types of defects can have a triplet ground state when embedded in the same layer, but in that case, the singlet and triplet are nearly degenerate [31]. Instead, when the defects belong to a different type ($C_B C_N$), the ground state is a singlet.

The relation between the spin state and the type of defect can be understood by looking at the energy of the defect levels within the fundamental gap of hBN. C_B has donor-like defect states (close to the conduction band). In contrast, C_N is acceptor-like (defect states closer to the valence band). This is illustrated in panels A and D of Fig. 5, where the configurations $C_B C_B-(a, 2)$ and $C_B C_N-(b, 2)$ are used as examples.

Panel A of Fig. 5 shows the occupied and empty defect levels of a $C_N C_B$ defect; they are located around C_N and C_B , respectively (Fig. 5B, C). This directly affects the total spin of the configurations with different types of defects, as it is energetically more favorable for the two extra electrons of the carbon to form a singlet and localize around the C_N defect.

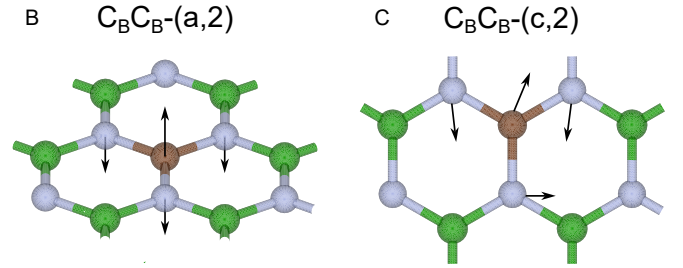
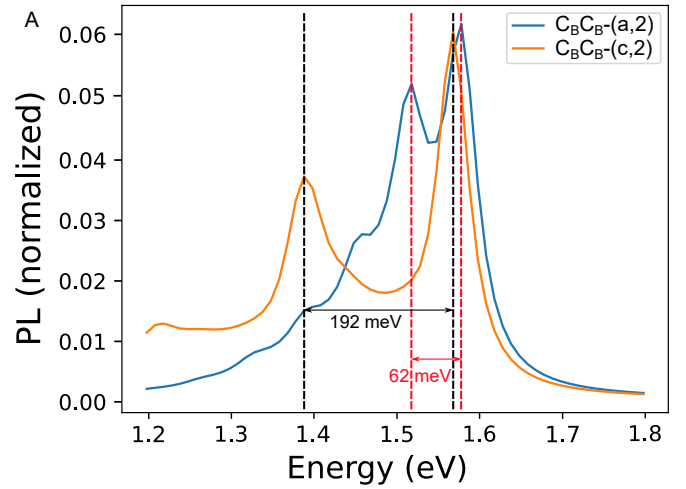


FIG. 4. (A) Photoluminescence spectra of $C_B C_B-(a, 2)$ (blue line) and $C_B C_B-(c, 2)$ (orange line) defects. The first phonon replica is highlighted as a vertical dashed line. It is 62 meV for $C_B C_B-(a, 2)$ and 192 meV for $C_B C_B-(c, 2)$. (B,C) Phonons with the largest partial Huang-Rhys factor, S_k . In panel B (C) the displacements are out-of-plane (in-plane). Only one layer is in the figures, as both are connected by inversion symmetry. In panel B (C), the C_3 symmetry is preserved (broken) by the C_B defects.

On the other hand, defects of the same species - such as $C_B C_B$ - are degenerate, and when close enough, their wavefunctions are linear combinations of both defect states, as shown in Fig. 5E-F. Also, there is a non-negligible overlap contribution on the B and N atoms along the line joining both C atoms. As the C_B states are degenerate, there is an important overlap of the wavefunctions of both occupied levels. This leads to an exchange energy, lowering the energy of the configuration when the total spin is a triplet. In contrast, when the total spin is a singlet, the exchange energy is null, making the energy of the singlet configuration higher than that of the triplet configuration.

B. Phonon sideband

When examining the electron-phonon coupling of the optical transition, the relevant phonon replicas are high-energy modes corresponding to bond stretching, typically associated with substitutional C defects [40]. Fig. 4A shows the defect $C_B C_B-(c, 2)$, whose phonon sideband is

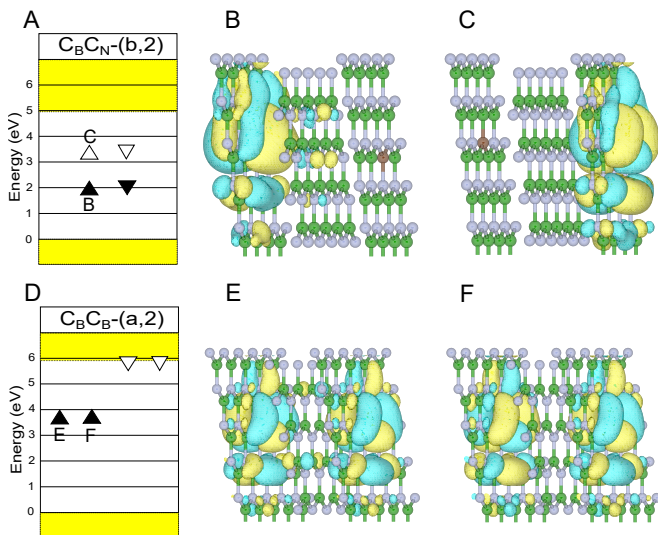


FIG. 5. In panels A and D, the energy levels of the defects $C_B C_N-(b,2)$ in its singlet state and $C_B C_B-(a,2)$ in its triplet state are shown, respectively. The letters label specific levels, depicted in panels B, C, E, and F. Panels B and C illustrate the wavefunctions of the occupied C_N and empty C_B energy levels, respectively. Panels E and F display the wavefunctions of the C_B occupied defect levels.

representative of most of the defects studied here. The optical excitation induces the transfer of one electron from a C atom to the other if the defect is $C_N C_B$, or from/to the C atom to the valence/conduction band if the defect is $C_X C_X$. Either way, the C–B and/or C–N bonds become weaker or stronger, resulting in a bond stretching: a high-energy localized longitudinal phonon.

However, there is one defect with a markedly different photoluminescence spectrum, $C_B C_B-(a,2)$, that is, the C_B defects are opposite to each other and separated by a N atom from an intermediate layer. This defect features a low-energy phonon replica shifted just 62 meV, see Fig. 4. In this defect, the C atoms are slightly displaced out of the plane (emulating a C–C repulsion) in the ground state, and the phonon associated with such distortion is responsible for the 62 meV phonon replica. In Fig. 4B, C, the phonon with the most relevant partial Huang-Rhys factor S_k is shown for two different dimers ($C_B C_B-(a,2)$ and $C_B C_B-(c,2)$). This behavior will be discussed in greater detail in the next section. To the best of our knowledge, there are a couple of reports of defects in hBN with a similar low-energy phonon replica, the so-called yellow emitters [69], but these emitters lack spin activity. Although we can discard $C_B C_B-(a,2)$ as yellow emitters, it is likely that the yellow emitters trigger an out-of-plane distortion, explaining their low-energy phonon replicas. The other report of SPEs with a similar PL was obtained in a hBN flake after a H_2 plasma treatment [70].

C. Weakly coupled spin pairs

Several reports of SPEs exhibit optically detected magnetic resonance (ODMR) with a very small zero-field splitting (ZFS) in the range of the MHz [20, 71–73]. Such a small ZFS can be associated with weakly coupled $S = 1/2$ defects [41] or defects with a triplet ground state but with a very small ZFS. Indeed, most $C_X C_X$ defects studied here are expected to have a small ZFS since both C atoms are separated by 0.4 – 1.0 nm and the ZFS decays as r^{-3} (in the vacuum). Note that a small ZFS is not incompatible with a large exchange energy, separating the singlet and triplet states. There is a general model aiming to explain the already mentioned ODMR results [42]. It mostly fits with the $C_N C_B-(d,h)$ defects studied here: donor-acceptor pairs, singlet ground state, C–C distance of ~ 1 nm. However, here, we show that weakly interacting triplet states could also be found in hBN multilayers. Particularly, the ODMR measured by Scholten *et al* [41] effectively behaves as spin 1/2 defects, as the authors demonstrated by Rabi oscillation measurements. Such behavior could occur in defects like the ones from our study, an actual triplet or singlet, but once the exchange energy becomes weaker, that is, when defects are further away. Going closer to the dissociation limit is not only computationally expensive but, more importantly, DFT is known for failing to describe such a limit.

V. CONCLUSIONS

Substitutional carbon defects are the most widely accepted explanation for the bright light emitters found in hBN. To the best of our knowledge, C-based defects have only been studied when in the same layer.

In this article, we show, by means of DFT calculations, that neutral C defects lying in different layers are also viable candidates to be associated with single emitters. If they form donor-acceptor-like pairs, they behave similarly to when residing in the same hBN layer: they are spinless, have a ZPL energy of ~ 1.6 eV, and their photoluminescence spectra feature well-defined high-energy phonon replicas.

However, if the two C atoms in different hBN layers are substituting N or B, they have a triplet ground state. It is separated by more than ~ 0.5 eV from the singlet state, making these defects spin-active above room temperature. Their ZPL can be larger than when the defects form donor-acceptor pairs, $E_{ZPL} \sim 1.6 - 2.2$ eV. Again, these defects present the typical high-energy phonon replicas in their photoluminescence spectra.

When two C_B atoms are on top of each other but separated by a hBN interlayer, we calculated a markedly different phonon sideband in the photoluminescence spectrum, with well-defined phonon replicas at ~ 60 meV. They correspond to out-of-plane rearrangement upon excitations. We are unaware of any measurement of such a spectrum for spin-active defects, but the so-called (spin-

less) yellow emitters have similar phonon replicas and could also correspond to out-of-plane distortions.

VI. COMPETING INTERESTS

The Authors declare no Competing Financial or Non-Financial Interests

VII. DATA AVAILABILITY

Input files for the most relevant calculations are provided as supplementary information. The remaining data is available from the corresponding author upon reasonable request.

VIII. AUTHOR CONTRIBUTIONS

I.C. and F.M. ran all the calculations. F.M. conceived the idea. C.C., A.E., and I.C. explained the stability of

the triplet state. All authors discussed the results and contributed to the manuscript's writing.

ACKNOWLEDGMENTS

This work was partially supported by Fondecyt Grants No. 1191353, 1220715, 1220366, 3240387, and 1221512, by the Center for the Development of Nanoscience and Nanotechnology CEDENNA AFB180001, and from Conicyt PIA/Anillo ACT192023. This research was partially supported by the supercomputing infrastructure of the NLHPC (ECM-02).

-
- [1] T. T. Tran, K. Bray, M. J. Ford, M. Toth, and I. Aharonovich, Quantum emission from hexagonal boron nitride monolayers, *Nature Nanotechnology* **11**, 37 (2016).
- [2] I. Aharonovich, J.-P. Tetienne, and M. Toth, Quantum emitters in hexagonal boron nitride, *Nano Letters* **22**, 9227 (2022).
- [3] Z. Qiu, K. Vaklinova, P. Huang, M. Grzeszczyk, K. Watanabe, T. Taniguchi, K. S. Novoselov, J. Lu, and M. Koperski, Atomic and electronic structure of defects in hbn: Enhancing single-defect functionalities, *ACS Nano* **18**, 24035 (2024).
- [4] N. Mendelson, D. Chugh, J. R. Reimers, T. S. Cheng, A. Gottscholl, H. Long, C. J. Mellor, A. Zettl, V. Dyakonov, P. H. Beton, et al., Identifying carbon as the source of visible single-photon emission from hexagonal boron nitride, *Nature materials* **20**, 321 (2021).
- [5] L. Weston, D. Wickramaratne, M. Mackoït, A. Alkauskas, and C. G. Van de Walle, Native point defects and impurities in hexagonal boron nitride, *Phys. Rev. B* **97**, 214104 (2018).
- [6] C. Linderälv, W. Wiczorek, and P. Erhart, Vibrational signatures for the identification of single-photon emitters in hexagonal boron nitride, *Phys. Rev. B* **103**, 115421 (2021).
- [7] M. Mackoït-Sinkevičienė, M. Maciaszek, C. G. Van de Walle, and A. Alkauskas, Carbon dimer defect as a source of the 4.1 eV luminescence in hexagonal boron nitride, *Applied Physics Letters* **115**, 212101 (2019), https://pubs.aip.org/aip/apl/article-pdf/doi/10.1063/1.5124153/13286483/212101_1_online.pdf.
- [8] X. Z. Du, J. Li, J. Y. Lin, and H. X. Jiang, The origin of deep-level impurity transitions in hexagonal boron nitride, *Applied Physics Letters* **106**, 021110 (2015), https://pubs.aip.org/aip/apl/article-pdf/doi/10.1063/1.4905908/14088224/021110_1_online.pdf.
- [9] R. Bourrellier, S. Meuret, A. Tararan, O. Stéphan, M. Kociak, L. H. G. Tizei, and A. Zobelli, Bright uv single photon emission at point defects in h-bn, *Nano Letters* **16**, 4317 (2016).
- [10] D. Wong, J. J. Velasco, L. Ju, J. Lee, S. Kahn, H.-Z. Tsai, C. Germany, T. Taniguchi, K. Watanabe, A. Zettl, F. Wang, and M. F. Crommie, *Nature Nanotechnology* **10**, 949 (2015).
- [11] O. Golami, K. Sharman, R. Ghobadi, S. C. Wein, H. Zadeh-Haghighi, C. Gomes da Rocha, D. R. Salahub, and C. Simon, *ab initio* and group theoretical study of properties of a carbon trimer defect in hexagonal boron nitride, *Phys. Rev. B* **105**, 184101 (2022).
- [12] M. Fischer, A. Sajid, J. Iles-Smith, A. Hötger, D. I. Miakota, M. K. Svendsen, C. Kastl, S. Canulescu, S. Xiao, M. Wubs, K. S. Thygesen, A. W. Holleitner, and N. Stenger, Combining experiments on luminescent centres in hexagonal boron nitride with the polaron model and ab initio methods towards the identification of their microscopic origin, *Nanoscale* **15**, 14215 (2023).
- [13] M. Maciaszek and L. Razinkovas, Blue quantum emitter in hexagonal boron nitride and a carbon chain tetramer: a first-principles study, *ACS Applied Nano Materials* **7**, 18979 (2024).
- [14] M. Neumann, X. Wei, L. Morales-Inostroza, S. Song, S.-G. Lee, K. Watanabe, T. Taniguchi, S. Götzinger, and Y. H. Lee, Organic molecules as origin of visible-range single photon emission from hexagonal boron nitride and mica, *ACS Nano* **17**, 11679 (2023).
- [15] C. Cholsuk, S. Suwanna, and T. Vogl, Comprehensive scheme for identifying defects in solid-state quantum systems, *The Journal of Physical Chemistry Letters* **14**, 6564 (2023).

- [16] A. Kirchhoff, T. Deilmann, P. Krüger, and M. Rohlfling, Electronic and optical properties of a hexagonal boron nitride monolayer in its pristine form and with point defects from first principles, *Phys. Rev. B* **106**, 045118 (2022).
- [17] G. Cassabois, P. Valvin, and B. Gil, Hexagonal boron nitride is an indirect bandgap semiconductor, *Nature Photonics* **10**, 262 (2016).
- [18] R. J. P. Román, F. J. R. C. Costa, A. Zobelli, C. Elias, P. Valvin, G. Cassabois, B. Gil, A. Summerfield, T. S. Cheng, C. J. Mellor, P. H. Beton, S. V. Novikov, and L. F. Zagonel, Band gap measurements of monolayer h-BN and insights into carbon-related point defects, *2D Materials* **8**, 044001 (2021).
- [19] A. Gottscholl, M. Diez, V. Soltamov, C. Kasper, A. Sperlich, M. Kianinia, C. Bradac, I. Aharonovich, and V. Dyakonov, Room temperature coherent control of spin defects in hexagonal boron nitride, *Science Advances* **7**, 10.1126/sciadv.abf3630 (2021).
- [20] H. L. Stern, Q. Gu, J. Jarman, S. Eizagirre Barker, N. Mendelson, D. Chugh, S. Schott, H. H. Tan, H. Sirringhaus, I. Aharonovich, et al., Room-temperature optically detected magnetic resonance of single defects in hexagonal boron nitride, *Nature communications* **13**, 1 (2022).
- [21] M. Kianinia, S. White, J. E. Fröch, C. Bradac, and I. Aharonovich, Generation of spin defects in hexagonal boron nitride, *ACS Photonics* **7**, 2147 (2020).
- [22] S. Li, A. Pershin, G. Thiering, P. Udvarhelyi, and A. Gali, Ultraviolet quantum emitters in hexagonal boron nitride from carbon clusters, *The Journal of Physical Chemistry Letters* **13**, 3150 (2022).
- [23] X. Gao, S. Pandey, M. Kianinia, J. Ahn, P. Ju, I. Aharonovich, N. Shivaram, and T. Li, Femtosecond laser writing of spin defects in hexagonal boron nitride, *ACS Photonics* **8**, 994 (2021).
- [24] A. Acín, I. Bloch, H. Buhrman, T. Calarco, C. Eichler, J. Eisert, D. Esteve, N. Gisin, S. J. Glaser, F. Jelezko, S. Kuhr, M. Lewenstein, M. F. Riedel, P. O. Schmidt, R. Thew, A. Wallraff, I. Walmsley, and F. K. Wilhelm, The quantum technologies roadmap: A european community view, *New Journal of Physics* **20**, 080201 (2018).
- [25] P. Auburger and A. Gali, Towards ab initio identification of paramagnetic substitutional carbon defects in hexagonal boron nitride acting as quantum bits, *Phys. Rev. B* **104**, 075410 (2021).
- [26] S. Moon, J. Kim, J. Park, S. Im, J. Kim, I. Hwang, and J. K. Kim, Hexagonal boron nitride for next-generation photonics and electronics, *Advanced Materials* **35**, 2204161 (2023).
- [27] M. Kianinia, Z.-Q. Xu, M. Toth, and I. Aharonovich, Quantum emitters in 2d materials: Emitter engineering, photophysics, and integration in photonic nanostructures, *Applied Physics Reviews* **9**, 011306 (2022).
- [28] A. Çakan, C. Cholsuk, A. Gale, M. Kianinia, S. Paçal, S. Ateş, I. Aharonovich, M. Toth, and T. Vogl, Quantum optics applications of hexagonal boron nitride defects (2024), arXiv:2410.07712 [quant-ph].
- [29] C. Cholsuk, A. Çakan, S. Suwanna, and T. Vogl, Identifying electronic transitions of defects in hexagonal boron nitride for quantum memories, *Advanced Optical Materials* **12**, 2302760 (2024), <https://onlinelibrary.wiley.com/doi/pdf/10.1002/adom.202302760>
- [30] M. Esmann, S. C. Wein, and C. Antón-Solanas, Solid-state single-photon sources: Recent advances for novel quantum materials, *Advanced Functional Materials* **34**, 2315936 (2024).
- [31] F. Pinilla, N. Vásquez, I. Chacón, J. R. Maze, C. Cárdenas, and F. Muñoz, Spin-active single photon emitters in hexagonal boron nitride from carbon-based defects, *Physica Scripta* **98**, 095505 (2023).
- [32] M. Maciaszek, L. Razinkovas, and A. Alkauskas, Thermodynamics of carbon point defects in hexagonal boron nitride, *Phys. Rev. Materials* **6**, 014005 (2022).
- [33] Z. Benedek, R. Babar, Á. Ganyecz, T. zilvási, Ö. Legeza, G. Barcza, and V. Ivády, Symmetric carbon tetramers forming spin qubits in hexagonal boron nitride, *npj Computational Materials* **9**, 187 (2023).
- [34] N.-J. Guo, Y.-Z. Yang, X.-D. Zeng, S. Yu, Y. Meng, Z.-P. Li, Z.-A. Wang, L.-K. Xie, J.-S. Xu, J.-F. Wang, et al., Coherent control of an ultrabright single spin in hexagonal boron nitride at room temperature, arXiv preprint arXiv:2112.06191 (2021).
- [35] W. Liu, N.-J. Guo, S. Yu, Y. Meng, Z.-P. Li, Y.-Z. Yang, Z.-A. Wang, X.-D. Zeng, L.-K. Xie, Q. Li, J.-F. Wang, J.-S. Xu, Y.-T. Wang, J.-S. Tang, C.-F. Li, and G.-C. Guo, Spin-active defects in hexagonal boron nitride, *Materials for Quantum Technology* **2**, 032002 (2022).
- [36] C. Qian, V. Villafañe, M. Schalk, G. V. Astakhov, U. Kentsch, M. Helm, P. Soubelet, N. P. Wilson, R. Rizzato, S. Mohr, A. W. Holleitner, D. B. Bucher, A. V. Stier, and J. J. Finley, Unveiling the zero-phonon line of the boron vacancy center by cavity-enhanced emission, *Nano Letters* **22**, 5137 (2022).
- [37] A. Gottscholl, M. Kianinia, V. Soltamov, S. Orlinskii, G. Mamin, C. Bradac, C. Kasper, K. Krambrock, A. Sperlich, M. Toth, I. Aharonovich, and V. Dyakonov, Initialization and read-out of intrinsic spin defects in a van der waals crystal at room temperature, *Nature Materials* **19**, 540 (2020).
- [38] P. Huang, M. Grzeszczyk, K. Vaklinova, K. Watanabe, T. Taniguchi, K. S. Novoselov, and M. Koperski, Carbon and vacancy centers in hexagonal boron nitride, *Phys. Rev. B* **106**, 014107 (2022).
- [39] M. Almohammad, Z. Alemoush, J. Li, J. Y. Lin, and H. X. Jiang, Carbon-related donor-acceptor pair transition in the infrared in h-bn, *Applied Physics Letters* **124**, 102106 (2024).
- [40] C. Jara, T. Rauch, S. Botti, M. A. L. Marques, A. Norambuena, R. Coto, J. E. Castellanos-Águila, J. R. Maze, and F. Muñoz, First-principles identification of single photon emitters based on carbon clusters in hexagonal boron nitride, *J. P. Chem. A* **125**, 1325 (2021).
- [41] S. C. Scholten, P. Singh, A. J. Healey, I. O. Robertson, G. Haim, C. Tan, D. A. Broadway, L. Wang, H. Abe, T. Ohshima, M. Kianinia, P. Reineck, I. Aharonovich, and J.-P. Tetienne, Multi-species optically addressable spin defects in a van der waals material, *Nature Communications* **15**, 6727 (2024).
- [42] I. O. Robertson, B. Whitefield, S. C. Scholten, P. Singh, A. J. Healey, P. Reineck, M. Kianinia, D. A. Broadway, I. Aharonovich, and J.-P. Tetienne, A universal mechanism for optically addressable solid-state spin pairs (2024), arXiv:2407.13148 [cond-mat.med-hall].
- [43] J. Bhang, H. Ma, D. Yim, G. Galli, and H. Seo, First-principles predictions of out-of-plane group iv and v dimers as high-symmetry, high-spin defects in hexagonal boron nitride, *ACS Applied Materials & Interfaces*

- 13**, 45768 (2021).
- [44] G. Kresse and J. Hafner, Ab initio molecular dynamics for liquid metals, *Phys. Rev. B* **47**, 558(R) (1993).
- [45] G. Kresse and J. Hafner, Ab initio molecular-dynamics simulation of the liquid-metal-amorphous-semiconductor transition in germanium, *Phys. Rev. B* **49**, 14251 (1994).
- [46] G. Kresse and J. Furthmüller, Efficiency of ab-initio total energy calculations for metals and semiconductors using a plane-wave basis set, *Comput. Mater. Sci.* **6**, 15 (1996).
- [47] G. Kresse and J. Furthmüller, Efficient iterative schemes for ab initio total-energy calculations using a plane-wave basis set, *Phys. Rev. B* **54**, 11169 (1996).
- [48] D. Amblard, G. D'Avino, I. Duchemin, and X. Blase, Universal polarization energies for defects in monolayer, surface, and bulk hexagonal boron nitride: A finite-size fragments *gw* approach, *Phys. Rev. Mater.* **6**, 064008 (2022).
- [49] M. Winter, M. H. E. Bousquet, D. Jacquemin, I. Duchemin, and X. Blase, Photoluminescent properties of the carbon-dimer defect in hexagonal boron-nitride: A many-body finite-size cluster approach, *Phys. Rev. Materials* **5**, 095201 (2021).
- [50] D. I. Badrtdinov, C. Rodriguez-Fernandez, M. Grzeszczyk, Z. Qiu, K. Vaklinova, P. Huang, A. Hampel, K. Watanabe, T. Taniguchi, L. Jiong, M. Potemski, C. E. Dreyer, M. Koperski, and M. Rösner, Dielectric environment sensitivity of carbon centers in hexagonal boron nitride, *Small* **19**, 2300144 (2023).
- [51] F. Pinilla, W. A. Muriel, J. Cabezas-Escases, I. Chacón, C. Cárdenas, and F. Muñoz, Manipulating the stacking in two-dimensional hexagonal boron nitride bilayers: Implications for defect-based single photon emitters, *ACS Applied Nano Materials* **7**, 6039 (2024).
- [52] S. M. Gilbert, T. Pham, M. Dogan, S. Oh, B. Shevitski, G. Schumm, S. Liu, P. Ercius, S. Aloni, M. L. Cohen, and A. Zettl, Alternative stacking sequences in hexagonal boron nitride, *2D Materials* **6**, 021006 (2019).
- [53] U. Herath, P. Tavazde, X. He, E. Bousquet, S. Singh, F. Muñoz, and A. H. Romero, Pyprocar: A python library for electronic structure pre/post-processing, *Comput. Phys. Commun.* **251**, 107080 (2019).
- [54] L. Lang, P. Tavazde, A. Tellez, E. Bousquet, H. Xu, F. Muñoz, N. Vasquez, U. Herath, and A. H. Romero, Expanding pyprocar for new features, maintainability, and reliability, *Computer Physics Communications* **297**, 109063 (2024).
- [55] K. Momma and F. Izumi, Vesta 3 for three-dimensional visualization of crystal, volumetric and morphology data, *Journal of applied crystallography* **44**, 1272 (2011).
- [56] J. Sun, A. Ruzsinszky, and J. P. Perdew, Strongly constrained and appropriately normed semilocal density functional, *Phys. Rev. Lett.* **115**, 036402 (2015).
- [57] T. Rauch, F. Munoz, M. A. L. Marques, and S. Botti, Defect levels from scan and mbj meta-gga exchange-correlation potentials, *Phys. Rev. B* **104**, 064105 (2021).
- [58] A. V. Krukau, O. A. Vydrov, A. F. Izmaylov, and G. E. Scuseria, Influence of the exchange screening parameter on the performance of screened hybrid functionals, *J. Chem. Phys.* **125**, 224106 (2006).
- [59] P. Deák, B. Aradi, T. Frauenheim, E. Jánzén, and A. Gali, Accurate defect levels obtained from the hse06 range-separated hybrid functional, *Phys. Rev. B* **81**, 153203 (2010).
- [60] W. Yang and P. W. Ayers, Foundation for the Δ scf approach in density functional theory (2024), arXiv:2403.04604 [physics.chem-ph].
- [61] Y. Jin, M. Govoni, G. Wolfowicz, S. E. Sullivan, F. J. Heremans, D. D. Awschalom, and G. Galli, Photoluminescence spectra of point defects in semiconductors: Validation of first-principles calculations, *Phys. Rev. Mater.* **5**, 084603 (2021).
- [62] J. Iwanski, K. P. Korona, M. Tokarczyk, G. Kowalski, A. K. Dabrowska, P. Tatarczak, I. Rogala, M. Bilska, M. Wojcik, S. Kret, A. Reszka, B. J. Kowalski, S. Li, A. Pershin, A. Gali, J. Binder, and A. Wyszomolek, Revealing polytypism in 2d boron nitride with uv photoluminescence (2024), arXiv:2405.19126 [cond-mat.mtrl-sci].
- [63] K. Reuter and M. Scheffler, Composition, structure, and stability of B_2O_3 as a function of oxygen pressure, *Physical Review B* **65**, 10.1103/PhysRevB.65.035406 (2001).
- [64] I. Tomaszewicz, The enthalpy of formation of hexagonal boron nitride, *Polish Journal of Chemistry* **Vol. 76 / nr 6**, 891–899 (2002).
- [65] M. C. Jr., NIST-JANAF thermochemical tables, monograph 9, Vol. 9 (American Chemical Society, 1998) pp. 1–1951.
- [66] A. Alkauskas, B. B. Buckley, D. D. Awschalom, and C. G. Van de Walle, First-principles theory of the luminescence lineshape for the triplet transition in diamond *nv* centres, *New J. Phys.* **16**, 073026 (2014).
- [67] R. Babar, I. A. Abrikosov, G. Barcza, and V. Ivády, Carbon-contaminated topological defects in hbn: a potential new class of single photon emitters, arXiv preprint arXiv:2403.00755 (2024).
- [68] P. Santra, S. Ghaderzadeh, M. Ghorbani-Asl, H.-P. Komsa, E. Besley, and A. V. Krasheninnikov, Strain-modulated defect engineering of two-dimensional materials, *npj 2D Materials and Applications* **8**, 33 (2024).
- [69] A. Kumar, C. Cholsuk, A. Zand, M. N. Mishuk, T. Matthes, F. Eilenberger, S. Suwanna, and T. Vogl, Localized creation of yellow single photon emitting carbon complexes in hexagonal boron nitride, *APL Materials* **11**, 071108 (2023).
- [70] Y. Chen, C. Li, S. White, M. Nonahal, Z.-Q. Xu, K. Watanabe, T. Taniguchi, M. Toth, T. T. Tran, and I. Aharonovich, Generation of high-density quantum emitters in high-quality, exfoliated hexagonal boron nitride, *ACS Applied Materials & Interfaces* **13**, 47283 (2021).
- [71] Y.-Z. Yang, T.-X. Zhu, Z.-P. Li, X.-D. Zeng, N.-J. Guo, S. Yu, Y. Meng, Z.-A. Wang, L.-K. Xie, Z.-Q. Zhou, Q. Li, J.-S. Xu, X.-Y. Gao, W. Liu, Y.-T. Wang, J.-S. Tang, C.-F. Li, and G.-C. Guo, Laser direct writing of visible spin defects in hexagonal boron nitride for applications in spin-based technologies, *ACS Applied Nano Materials* **6**, 6407 (2023).
- [72] N.-J. Guo, S. Li, W. Liu, Y.-Z. Yang, X.-D. Zeng, S. Yu, Y. Meng, Z.-P. Li, Z.-A. Wang, L.-K. Xie, R.-C. Ge, J.-F. Wang, Q. Li, J.-S. Xu, Y.-T. Wang, J.-S. Tang, A. Gali, C.-F. Li, and G.-C. Guo, Coherent control of an ultra-bright single spin in hexagonal boron nitride at room temperature, *Nature Communications* **14**, 2893 (2023).
- [73] N. Chejanovsky, A. Mukherjee, J. Geng, Y.-C. Chen, Y. Kim, A. Denisenko, A. Finkler, T. Taniguchi, K. Watanabe, D. B. R. Dasari, et al., Single-spin resonance in a van der waals embedded paramagnetic defect, *Nature materials* **20**, 1079 (2021).